Research Article

For reprint orders, please contact: reprints@futuremedicine.com

Nanomedicine

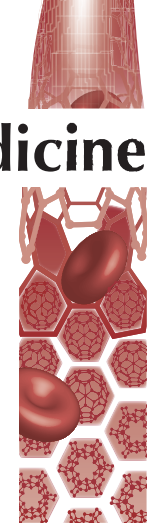

Evaluating cellular uptake of gold nanoparticles in HL-7702 and HepG2 cells for plasmonic photothermal therapy

Peng Wang[1], Qiang Wu[2], Fuyan Wang[3], Yaping Zhang[4], Liying Tong[1], Tao Jiang[1], Chenjie Gu[1], Shuiping Huang[1], Hongxi Wang[5], Shizhong Bu[3] & Jun Zhou*[,1]

[1]Faculty of Science, Institute of Photonics, Ningbo University, Ningbo 315211, Zhejiang, China

[2]Department of Mathematics, Physics & Electrical Engineering, Northumbria University, Newcastle upon Tyne, NE1 8ST, UK

[3]Zhejiang Provincial Key Laboratory of Pathophysiology School of Medicine, Ningbo University, Ningbo 315211, Zhejiang, China

[4]Department of Electrical & Electronic Engineering, University of Nottingham Ningbo China, Ningbo 315100, China

[5]Science Department, Zhenhai High School of Zhejiang, Ningbo 315200, China

*Author for correspondence: Tel.:+86 574 8760 0794; Fax: +86 574 8760 0744; zhoujun@nbu.edu.cn

Aim: A novel methodology is provided to quantitatively measure the gold (Au) mass internalized in a cell for effective implementation of plasmonic photothermal therapy (PPTT). **Materials & methods:** The cellular uptake of 4-mercaptobenzoic acid-labeled Au nanoparticles (NPs) is investigated via Raman mapping and inductively coupled plasma-mass spectrometry and the efficiency of *in vitro* PPTT is evaluated. **Results & conclusion:** The cellular uptake is strongly affected by the size of the Au NPs, concentration of the Au NPs, incubation time and cell type. By optimizing the experimental parameters, the results show that a significant damage is caused to the HepG2 cells and slight harm is caused to the HL-7702 cells during PPTT. This demonstrates a high potential for developing effective photothermal therapy for tumor tissues.

Graphical abstract:

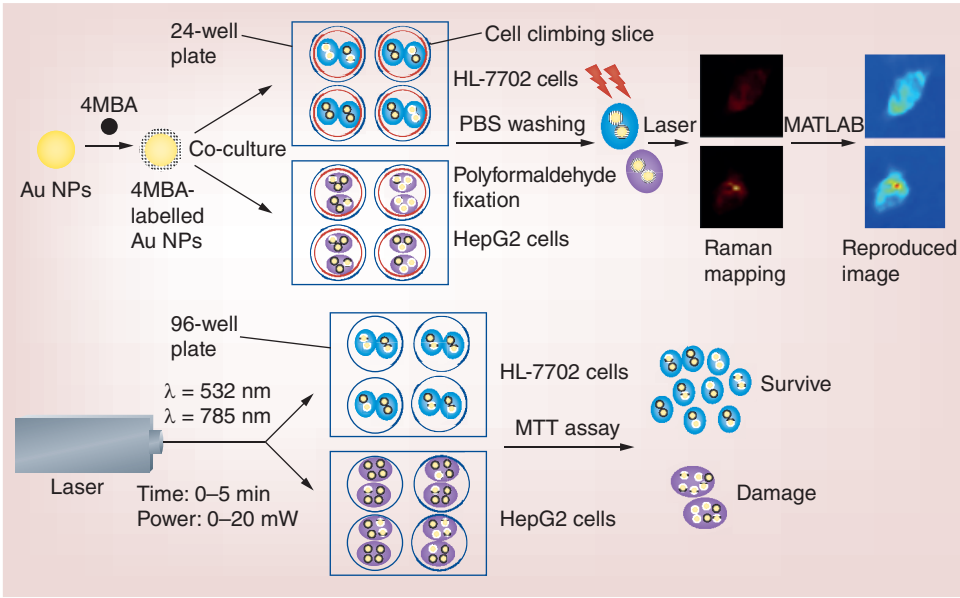

A novel method is proposed for quantifying the Raman intensity as a function of gold mass in a single cell based on the Raman mapping and inductively coupled plasma-mass spectrometry techniques. And a high-efficiency plasmonic photothermal therapy has also been achieved by adjusting the laser wavelength, laser power and exposure time, resulting in most of the HL-7702 cells survive, whereas most of the HepG2 cells get damaged.

Future Medicine

First draft submitted: 16 April 2018; Accepted for publication: 16 July 2018; Published online: 28 September 2018

Keywords: cellular uptake • cytotoxicity • gold nanoparticles • human hepatocellular carcinoma cell lines (HepG2) • human hepatic immortalized cell lines (HL-7702) • ICP-MS • plasmonic photothermal therapy • Raman mapping • surface enhanced Raman scattering (SERS).

Plasmonic photothermal therapy (PPTT) has attracted an increasing attention as a noninvasive method for its application in the treatment of cancer [1,2]. In the process of PPTT, when the plasmonic nanoparticles (NPs) internalized in the tumor tissues are irradiated by a laser, the oscillation of electrons in the conduction band of the plasmonic NPs, in other words, the surface plasmon oscillation, is excited, thus simultaneously absorbing and scattering the laser light and resulting in the conversion of the absorbed light to heat to kill the cancer cells [3–5]. To achieve high-efficiency PPTT, various functional plasmonic NPs have been developed in the past [6,7]. For example, synthesized polygonal gold (Au) NPs were bonded with vancomycin as photothermal agents to kill the bacteria by irradiating of near-infrared (NIR) light [8]. Au nanorods conjugated with polydopamine were coated by EGF receptor antibodies for cancer cell-targeted imaging and photothermal therapy by NIR light [9]. Biodegradable liposome–Au NPs were used to ablate the mouse tumor xenograft by illuminating with an NIR laser of 750 nm wavelength [10]. In ideal PPTT, the cancer cells are expected to be destroyed completely with the normal cells surviving without any damage. To achieve this objective, a direct solution is the internalization of more plasmonic NPs into the cancer cells and fewer plasmonic NPs into the normal cells, which will excite strong oscillation of surface plasmon polaritons in the cancer cells, resulting in a significant conversion of light to heat to damage the cancer cells. Therefore, it is important to investigate the cellular uptake processes of plasmonic NPs for both cancer and normal cells.

Various advanced technologies have been used to investigate the cellular uptake of plasmonic NPs [11]. Dark field microscopy and transmission electron microscopy (TEM) were combined to quantify the number of Au NPs and locate the Au NPs in the cell [12]. A focused ion beam/scanning electron microscopy (SEM) slice and view approach was presented to systematically analyze the cellular uptake of silver NPs in an individual human macrophage [13]. Multiple techniques such as photon cross-correlation spectroscopy, lactate dehydrogenase, Alamar blue assay and TEM were adopted to assess the toxicity and cellular uptake of Ag NPs in human lung cells (BEAS-2B) [14]. However, these sophisticated techniques require extensive and time-consuming sample preparation for quantifying the cellular uptake of plasmonic NPs [15]. As a highly sensitive elemental analysis technology, inductively coupled plasma-mass spectrometry (ICP-MS) is usually used for accurately determining the mass of metal or metal oxide NPs internalized in cells [16]. In addition, as a noninvasive imaging technique, Raman mapping has been widely applied in molecular detection and cell imaging with a high spatial resolution [17]. Clearly, by combining the advantages of ICP-MS and Raman mapping, the process of cellular uptake in cells can be quantitatively measured, which is important for developing controllable and highly efficient PPTT.

In our work, the cancerous (HepG2) hepatic cells and normal (HL-7702) are respectively chosen as typical cancer sample and a control sample because of the serious threat of liver cancer. And 4-mercaptobenzoic acid (4MBA) as Raman molecule was linked with the Au NPs to form 4MBA-labeled Au NPs, due to its distinct Raman characteristic and low cytotoxicity [18]. The surface-enhanced Raman scattering (SERS) signal of 4MBA was used to evaluate the cellular uptake for HL-7702 and HepG2 cells by combining of Raman mapping and ICP-MS techniques for achieving high-efficiency PPTT. During the co-culture period of the cells and 4MBA-labeled Au NPs, we found that the Au mass in the cells increased with an increasing incubation time and size and concentration of the Au NPs. The Au mass internalized in the HepG2 cells was much larger than that in the HL-7702 cells. Particularly, when the size and concentration of the Au NPs were 35 nm and 50 μg/ml, respectively, the ratio of the Au mass in the HL-7702 cells to that in the HepG2 cells reached an optimal value of 9.08 for an incubation time of 16 h. Moreover, the cytotoxicity of the Au NPs was evaluated using methyl thiazolyl tetrazolium (MTT) assays for analyzing the cell viabilities of the HL-7702 and HepG2 cells. Subsequently, *in vitro* PPTT experiments were conducted using the different laser wavelengths, laser powers and exposure times. Our results showed that under the optimal values of 566 W/cm^2 of irradiated intensity, 4 min of exposure time and 532 nm of laser wavelength, 65% HepG2 cells were killed, whereas 73.8% HL-7702 cells still survived. This demonstrated that cellular uptake of Au NPs was the key for realizing high-efficiency PPTT for the *in vivo* treatment of tumors.

Materials & methods

Materials

Tetrachloroauric acid ($HAuCl_4 \cdot 3H_2O$), MTT, dimethyl sulfoxide, paraformaldehyde and phosphate buffer solution (PBS; pH = 7.0) were purchased from Sigma-Aldrich Corporation, USA. Trisodium citrate dehydrate ($C_6H_5Na_3O_7 \cdot 2H_2O$) was purchased from Tianjin Bodi Chemical Reagents Co. Ltd, China. 4MBA was obtained from Tokyo Chemical Industry Co. Ltd, Japan. Human hepatic immortalized cell lines (HL-7702) and human hepatocellular carcinoma cell lines (HepG2) were obtained from the Shanghai Cell Bank of the Chinese Academy of Sciences, China. Dulbecco's modified Eagle's medium, fetal bovine serum, penicillin and streptomycin were purchased from Shanghai Excell Biotechnology Co. Ltd, China. 24 well plates and cell climbing slices were purchased from Ningbo Hangjing Biotechnology Co. Ltd, China. Pancreatin was purchased from Shanghai Biyun Tian Biotechnology Co. Ltd, China. Milli-Q water (resistivity of 18.2 $M\Omega \cdot cm^{-1}$) was used for the preparation of all the solutions. All the glassware used were cleaned by freshly prepared aqua regia solution (HCl: HNO_3; 3:1) before the synthesis of the NPs. In addition, all the solutions were sterilized prior to the cell experiments.

Synthesis of citrate-capped gold nanoparticles labeled with 4-mercaptobenzoic acid

Au NPs were synthesized using Frens' modified method [19]. Initially, 500 ml of de-ionized water was equally injected into five Erlenmeyer flasks; then 1 ml of $HAuCl_4$ (25.38 mM/l) was added to each flask. Second, the $HAuCl_4$ solutions in the flasks were heated to boiling; then, different amounts of sodium citrate (2, 1, 0.9, 0.7 and 0.5 ml, 0.039 M/l) were injected separately into the flasks with vigorous agitation for 20 min. Finally, the color of the solutions changed from dark blue to wine red, in other words, different sizes of Au NPs (20, 30, 35, 45 and 60 nm) were synthesized. After cooling to 20°C, the as-prepared Au NP solutions (2 ml) were centrifuged at 10,000 rpm for 20 min and the precipitates of the Au NPs were re-dispersed in 2 ml of de-ionized water.

The modification of Au NPs was performed with 4MBA. Briefly, 20 µL of 4MBA (10 mM/l) was separately added to the above purified Au NP solutions under stirring and the mixed solutions were agitated for 8 h. Then the resultant solutions were centrifuged at 10,000 rpm for 20 min to remove unbound 4MBA molecules. Finally, the sediments were re-dispersed in 2 ml of de-ionized water to form the 4MBA-labeled Au NP solutions to be used in the subsequent experiments.

Cell culture

Both the HL-7702 and HepG2 cells were cultured in a regular growth medium composed of Dulbecco's modified Eagle's medium supplemented with 10% fetal bovine serum and 1% penicillin/streptomycin at 37°C in a humidified environment containing 5% CO_2.

Quantification of gold mass & Raman intensity

First, the HL-7702 and HepG2 cells were separately seeded on 24-well plates at a density of 1×10^5 cells/well and then, the cells were cultured for 24 h to achieve the logarithmic growth of the cells. Second, 200 µl of 4MBA-labeled Au NPs solution was added to each well of the 24-well plates and then the cells were incubated for 2, 4, 6, 8, 12, 16, 20 and 24 h, respectively. Next, the mixture medium in each well was pipetted and the cell climbing slice was washed twice by PBS. Subsequently, 200 µl of pancreatin (2000 BAEE u/ml) was injected into each well to digest the cells for 2 min and 20 µ of the cell solution was pipetted for cell counting using a cytometer. Last, the cells remaining in the 24-well plates were fixed by 0.4% paraformaldehyde (100 µl/well) for 30 min and dried at 20°C.

The quantifying relation between Au mass and Raman intensity of 4MBA in a single cell was obtained by the following steps. First, Raman spectra of the cell samples were measured by the scanning near-field optical microscope (SNOM) system with the parameters of 633 nm wavelength, 50 mW power and 2s integration time. Raman mapping images were obtained by scanning the cell samples and the integral of the Raman peaks at 1393 or 1576 cm^{-1} was recorded as the intensity of each pixel. Next, the Raman mapping image corresponding to the Raman peaks at 1393 cm^{-1} was reproduced by our self-written MATLAB program to obtain the cellular outlines with coordinates. Subsequently, from the Raman mapping image corresponding to the Raman peaks at 1576 cm^{-1}, the total Raman intensities in every cell were obtained by summing the Raman intensities of all the pixels in the cellular outlines. Next, the sum of the total Raman intensities in every cell was divided by the total number of cells in the image to obtain the average Raman intensity in a single cell. In addition, after the cell climbing slice was dissolved by aqua regia solution, the Au mass in the cells was measured by ICP-MS. Then, the measured Au mass

10.2217/nnm-2018-0126

was divided by the number of cells to obtain the Au mass per cell. Finally, for the HL-7702 and HepG2 cells, we set the relation between the Au mass per cell and average Raman intensity of the peaks at 1576 cm^{-1}.

Cellular uptake of gold NPs

The cellular uptake of the Au NPs was investigated by varying their size and concentration during the incubation of the cells. First, the HL-7702 and HepG2 cells on the 24-well plates were incubated with different diameters of Au NPs (200 µl, 50 µg/ml) for 24 h. Then, by same steps described in the previous section, the variation in the Au mass per cell was obtained from the average Raman intensity of the peaks at 1576 cm^{-1} for the different sizes of Au NPs. Second, the HL-7702 and HepG2 cells on the 24-well plates were incubated with different concentrations of Au NPs (200 µl, 12.5, 25, 50, 100 and 200 µg/ml) for 24 h and the variation in the Au mass per cell dependent on the concentration of the Au NPs was obtained. Instantly, the cellular uptake of the Au NPs in the HL-7702 and HepG2 cells was analyzed to determine the optimal size of the Au NPs, concentration of the Au NPs and incubation time for further experiments.

Cytotoxicity

The cytotoxicity of the Au NPs exposed to HL-7702 and HepG2 cells was determined using the MTT assay [20–22]. First, the HL-7702 and HepG2 cells in the logarithmic phase were separately seeded on a 96-well plate at a density of 2×10^4 cells/well as test samples. Then the cells were incubated for 12 h for the adherent growth of the cells. Second, 40 µl of Au NPs were separately added to each well and incubated for 16 h. Similar to the above program, the HL-7702 and HepG2 cells were incubated in Au NP-free media as the control samples. Next, 15 µl of the MTT reagent (3.5 mg/ml) was separately added to the test and control samples and all the cells were continuously incubated for 6 h at 37°C. After the mixed solutions were pipetted from the 96-well plate, 150 µl of dimethyl sulfoxide were added in each well to dissolve formazan crystals. Then, the 96-well plate was shaken by a swing bed for 10 min at 37°C. Finally, the absorbance of the solution in each well was measured by a microplate reader at 570 nm for evaluating the cell viability of the HL-7702 and HepG2 cells or cytotoxicity of the Au NPs.

Plasmonic photothermal therapy

Experimentally, different laser powers, irradiation times and wavelengths were used to investigate their effects on cell viability for achieving high-efficiency PPTT. The experimental procedure is described in the following steps. First, HL-7702 and HepG2 cells were seeded in a 96-well plate at a density of 2×10^4 cells/well and incubated with Au NPs for 16 h. Second, the 96-well plate was irradiated by a laser beam with a focus spot diameter of 60 µm and then the irradiated cells were used as test samples, whereas the other cells away from the irradiation were used as control samples. Here, the laser wavelengths were 532 and 785 nm. Concretely, considering the laser wavelength of 532 nm as an example, the HL-7702 and HepG2 cells were irradiated by different powers (4, 8, 12, 16 and 20 mW) for 3 min and then the cell viability was measured by an MTT assay. Moreover, by analyzing the cell viability, the optimal power was chosen for obtaining the largest difference between the cell viabilities of the HL-7702 and HepG2 cells. Similarly, another group of HL-7702 and HepG2 cells was irradiated by a laser with different exposure times (1, 2, 3, 4 and 5 min), and then their cell viabilities were measured to determine the optimal exposure time for the largest difference between the cell viabilities of the HL-7702 and HepG2 cells.

Similarly, for the laser wavelength of 785 nm, the optimal power and exposure time were also obtained for the largest difference between the cell viabilities of the HL-7702 and HepG2 cells.

Instruments

The SEM images were obtained by performing field-emission scanning electron microscopy (SU-70, Hitachi, Japan) at an accelerating voltage of 5 kV. The UV–Visible absorption spectra were measured by a spectrometer (TU1901, Pgeneral, China). Dynamic light scattering (DLS) measurements were performed with the nanoparticle size analyzer (Zetasizer Nano S90, Malvern, UK). The thermogravimetric data was measured by a thermogravimetric analyzer (SII TG/DTA 7300, Exstar, Japan). Raman mapping images were obtained by a Raman spectrometer (MS 3504i) which belongs to a part of a SNOM system (Ntegra Spectra, NT-MDT, Russia), with semiconductor laser of 633 nm and 50 mW, 100 × objective lens (NA = 0.7), Al-coated grating of 1800 lines/mm and charge coupled device detector (2048 × 2048 pixels). The Au mass was measured by ICP-MS (NexION 300X, PerkinElmer, USA). The absorbance of the cells was recorded using a microplate reader (Dojindo, Tokyo, Japan) at 570 nm.

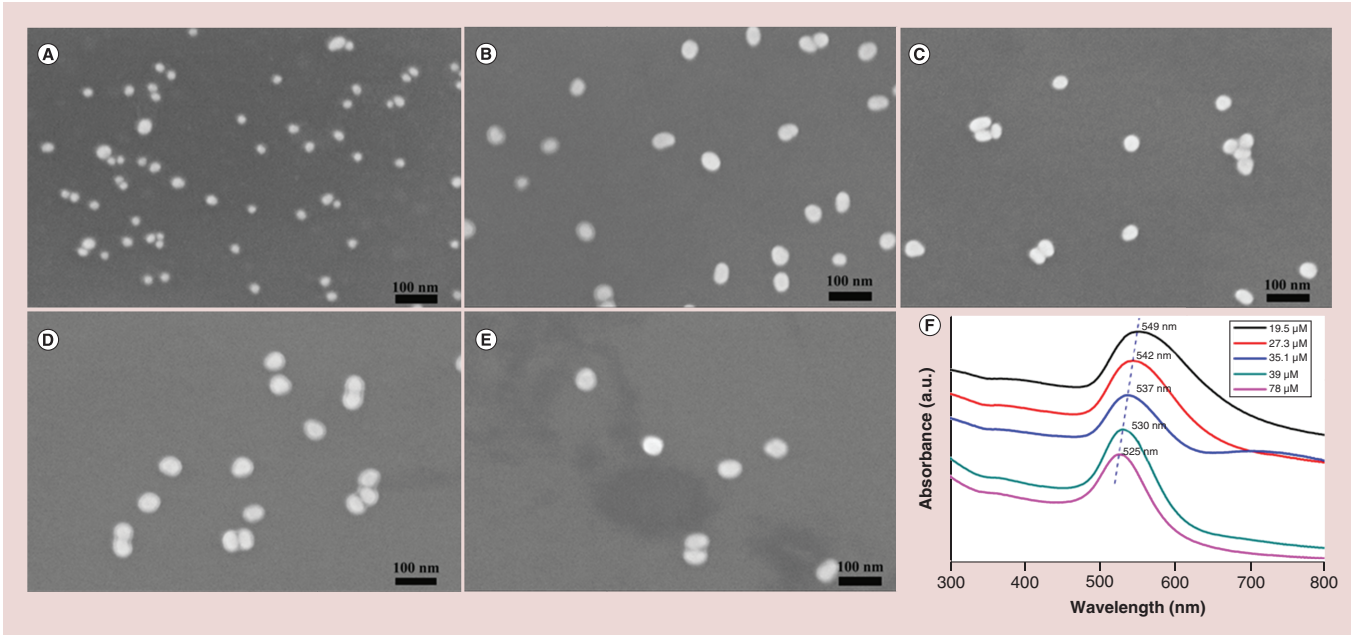

Figure 1. SEM images of the Au NPs with different sizes. (A) 20 nm; **(B)** 30 nm; **(C)** 35 nm; **(D)** 45 nm and **(E)** 60 nm, which were prepared with sodium citrate of 78, 39, 35.1, 27.3 and 19.5 μM, respectively; **(F)** UV-visible spectra of the Au NP solutions prepared with above amounts of sodium citrate.
Au NP: Gold nanoparticle; SEM: Scanning electron microscopy.

The PPTT experiments were conducted individually with two lasers of 532 and 785 nm wavelengths (Raman & FL-1705, SPL Photonics, China).

Results

Characterization of gold NPs

Various sizes of citrate-capped Au NPs were synthesized by adjusting the ratio of the citrate to $HAuCl_4$, in reference to Frens' method [19]. The SEM images and absorption spectra of the Au NPs are shown in Figure 1. It is found from Figure 1A–E that the average sizes of the Au NPs are approximately 20, 30, 35, 45 and 60 nm, respectively, so that the size of the Au NPs increase with the decrease in sodium citrate. Figure 1F displays that the absorption peak of the Au NPs shifts to longer wavelengths as their size increases. By comparing the absorption spectra (Figure S1 in Supplementary material) of Au NPs and 4MBA-labeled Au NPs, it is seen that their absorption peaks have only little red-shifts after the 4MBA was linked on the surfaces of Au NPs for same sizes of Au NPs. It presents the 4MBA-labeled Au NPs have larger sizes than that of the original Au NPs. Moreover, as the narrow size distributions determined by (DLS) (Figure S2 in Supplementary material), the average diameters of Au NPs listed in Table S1 in Supplementary materials are consisted with the measurement of SEM images (Figure 1[A–E]).

Quantifying gold mass in cells

As described in the experiment section, Raman mapping and ICP-MS were used to quantify the Au mass in the HL-7702 and HepG2 Cells. As an example, the SERS spectrum of the 4MBA-labeled Au NPs and the Raman spectrum of HepG2 cell are shown in Figure 2. In Figure 2A, it is clear that the peaks at 1073 and 1576 cm^{-1} originate from the in-plane ring breathing mode coupled with aromatic ring ν(C-C) vibration mode of the 4MBA molecules. In Figure 2B, the peaks at 1364 and 1393 cm^{-1} are ascribed to the bending vibration of CH_2 of tryptophan and vibration of CH_3 of lipids in the cells, respectively [23,24]. In addition, the Raman mapping images of the 4MBA-labeled Au NPs and HepG2 cells were recorded using the SNOM system, which are presented in Figure 3A and C, respectively. In Figure 3A, the bright spots correspond to the strong signal of the peaks at 1576 cm^{-1}, which indicates the aggregation of more 4MBA-labeled Au NPs [25,26]. In Figure 3C, the outlines of the HepG2 cells are very clear owing to the presence of the CH_3 bonds in all the cells. Furthermore, the self-compiled MATLAB program was used to convert Figure 3A and C into the reproduced images with coordinates Figure 3B

10.2217/nnm-2018-0126

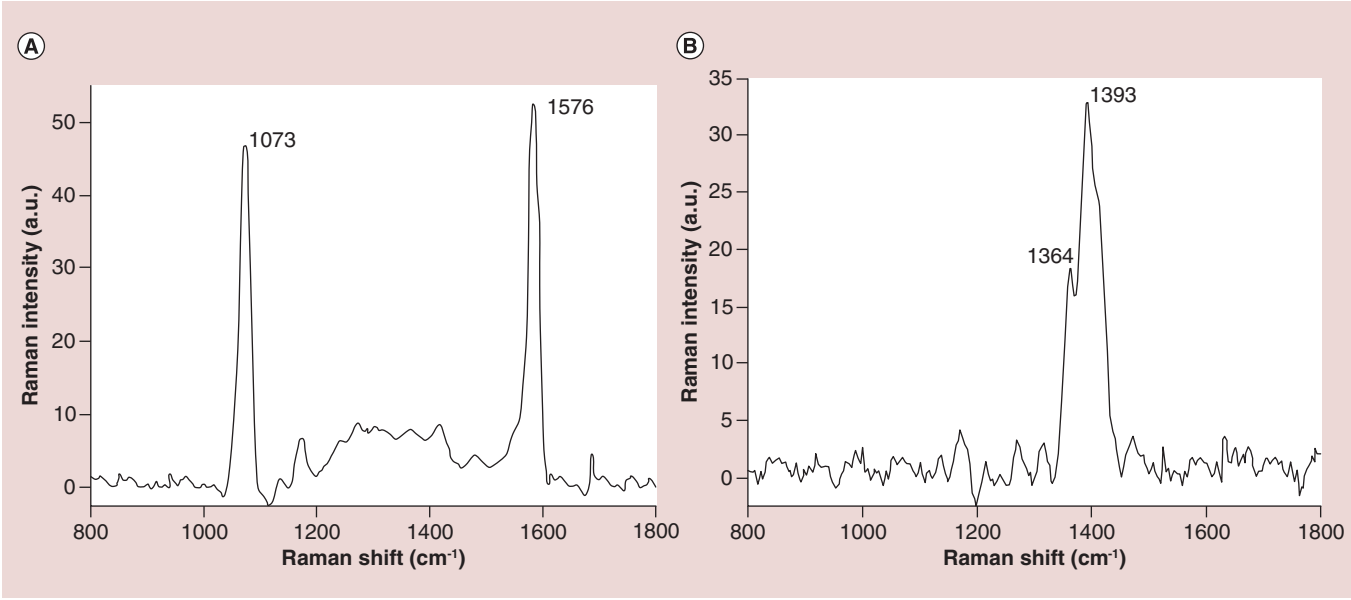

Figure 2. SERS and Raman spectra. (A) SERS spectrum of 4MBA-labeled Au NPs with a size of 35 nm and **(B)** Raman spectrum of HepG2 cell.
Au NP: Gold nanoparticle; 4MBA: 4-mercaptobenzoic acid; SERS: Surface-enhanced Raman scattering.

and D, respectively. That is, Figure 3B and D are the digital images of Raman mapping images. Thus, according to the methodology described in the experiment section, by simply overlapping Figure 3B and D, the average Raman intensity of the 4MBA molecules in a single HepG2 cell is acquired accurately to be 30500 (a. u.). Similarly, the average Raman intensities corresponding to the other incubation times were also obtained and are shown in Figure 4(A). The average Raman intensity of the 4MBA molecules in a single HL-7702 cell is displayed in Figure 4B. In Figure 4, it is seen that the average Raman intensity increases with the increase in the incubation time for both the cells. Simultaneously, the Au mass in a single HL-7702 cell and single HepG2 cell was measured by ICP-MS. The Au mass in single HL-7702 and HepG2 cells as a function of the average Raman intensity of the peaks at 1576 cm^{-1} are separately presented in Figure 5A and B, where each curve can be formulated by

$$y = A_1 + \frac{A_2 - A_1}{1 + 10^{[(x_0 - x)*p]}}$$

where y is the Au mass per cell, x is the average Raman intensity of the peaks at 1576 cm^{-1} and A_1, A_2, x_0, and p are constants as listed in Table 1.

Effect of cellular uptake

The cellular uptake or cell endocytosis of NPs follows the interaction process of the NPs and cell membrane, for which the NPs are enclosed by a portion of the cell membranes and introduced to the membrane-bound vesicle of the cells [27–30]. First, Au NPs of various sizes and concentrations were incubated with HL-7702 and HepG2 cells for 24 h, respectively. Then the Au mass endocytosed into single HL-7702 and HepG2 cells was obtained by measuring the average Raman intensity of the 4MBA-labeled Au NPs in the single cells with different incubation times. Next, with a simple conversion, the number of Au NPs internalized in the HL-7702 and HepG2 cells were easily obtained and are presented in Figure 6 A–B, respectively. From Figure 6, it is clear the number of Au NPs in both the cells increase with the increase in the incubation time. Here, considering the unstable cellular uptake of Au NPs, collecting data begins from 2 h, due to the fast exocytosis of Au NPs below 2 h incubation time [27]. And compared with the HL-7702 cells, the internalization of the Au NPs in the HepG2 cells rapidly saturates, reaching a plateau. Particularly, the number of Au NPs of 35 nm size is more than that of other Au NPs, after

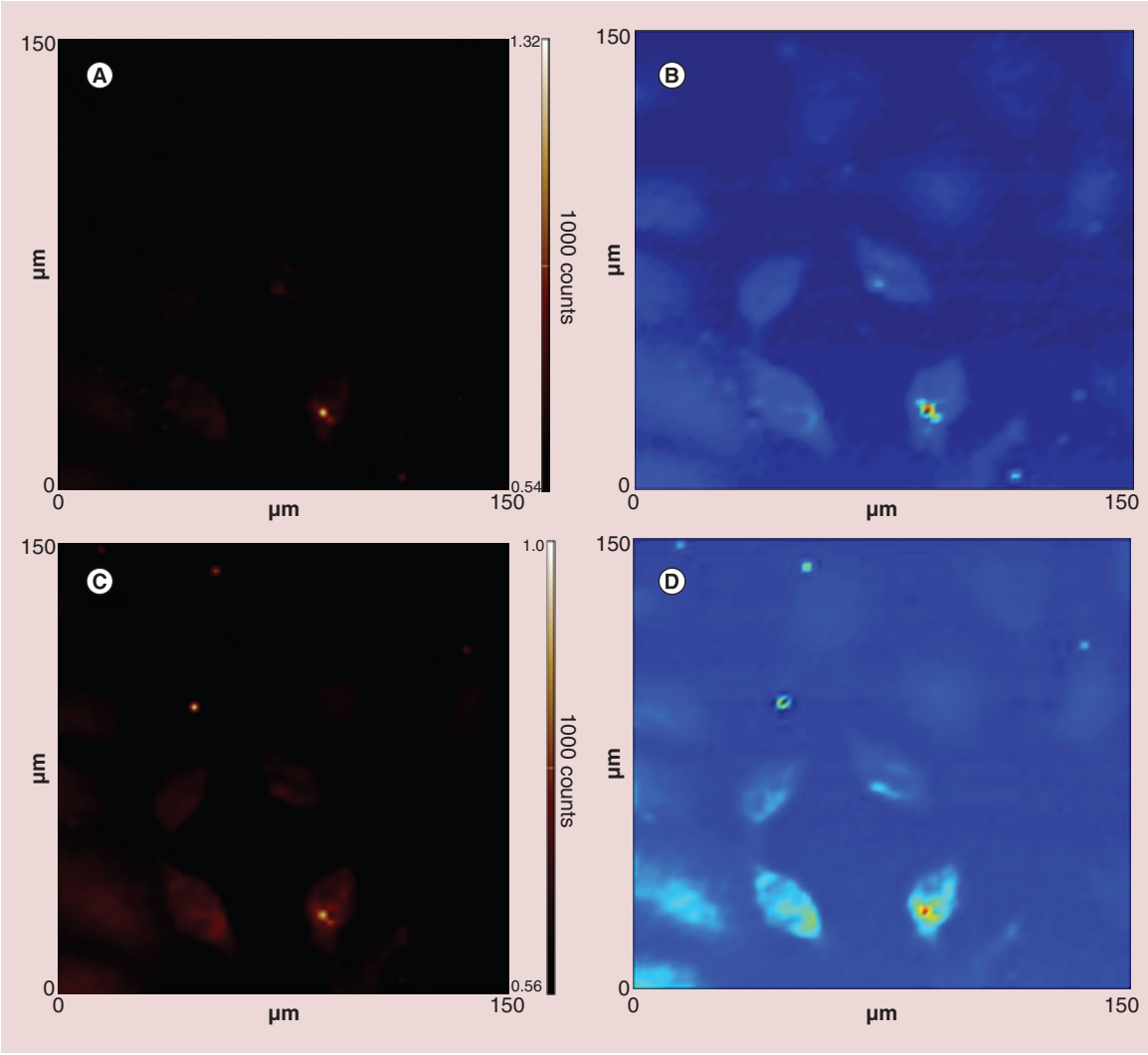

Figure 3. Raman mapping images and their reproduced images. Raman mapping images of **(A)** 4MBA-labeled gold nanoparticles and **(C)** HepG2 cells after incubation with Au NPs (35 nm, 50 μg/ml) for 16 h; **(B)** and **(D)** are the reproduced images of (A) and (C), respectively.
Au NP: Gold nanoparticle; 4MBA: 4-mercaptobenzoic acid.

Table 1. Parameters corresponding to each curve.

$$y = A_1 + \frac{A_2 - A_1}{1 + 10^{[(x_0 - x)*p]}}$$

Cell	Size	A_1	A_2	x_0	p	R^2
HL-7702	20 nm	0.00013	0.00039	548.132	0.08587	0.97014
	30 nm	0.00028	0.00149	555.133	0.10537	0.99295
	35 nm	0.00044	0.02394	616.703	0.02236	0.99177
	45 nm	0.00069	0.00284	548.575	0.08169	0.98358
	60 nm	0.00082	0.00649	551.127	0.08601	0.99630
HepG2	20 nm	-0.02518	0.00193	24310.720	284.826	0.96119
	30 nm	0.00358	0.00617	28299.168	234.543	0.97259
	35 nm	0.00563	0.01620	28939.480	422.784	0.98818
	45 nm	-0.12253	0.00555	25329.962	257.280	0.99319
	60 nm	-3.48358	0.01487	15350.820	1875.130	0.98451

10.2217/nnm-2018-0126

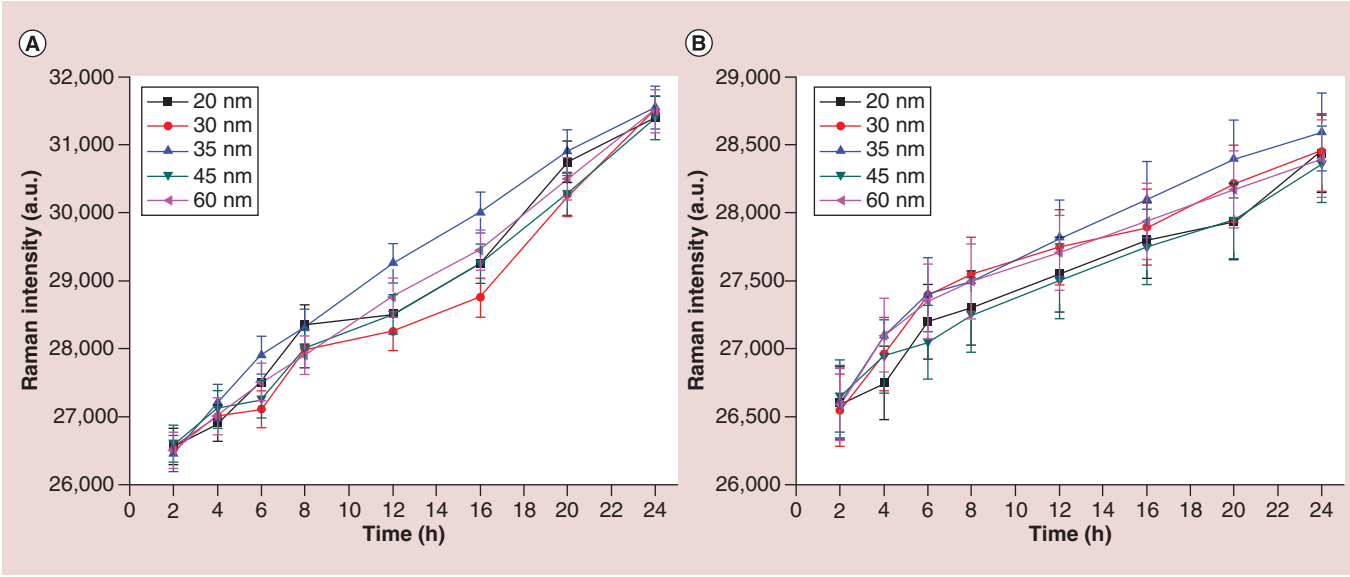

Figure 4. Average Raman intensity of 4MBA-labeled Au NPs as a function of the incubation time for cell. (A) Single HepG2 cell and **(B)** single HL-7702 cell.
Au NP: Gold nanoparticle; 4MBA: 4-mercaptobenzoic acid.

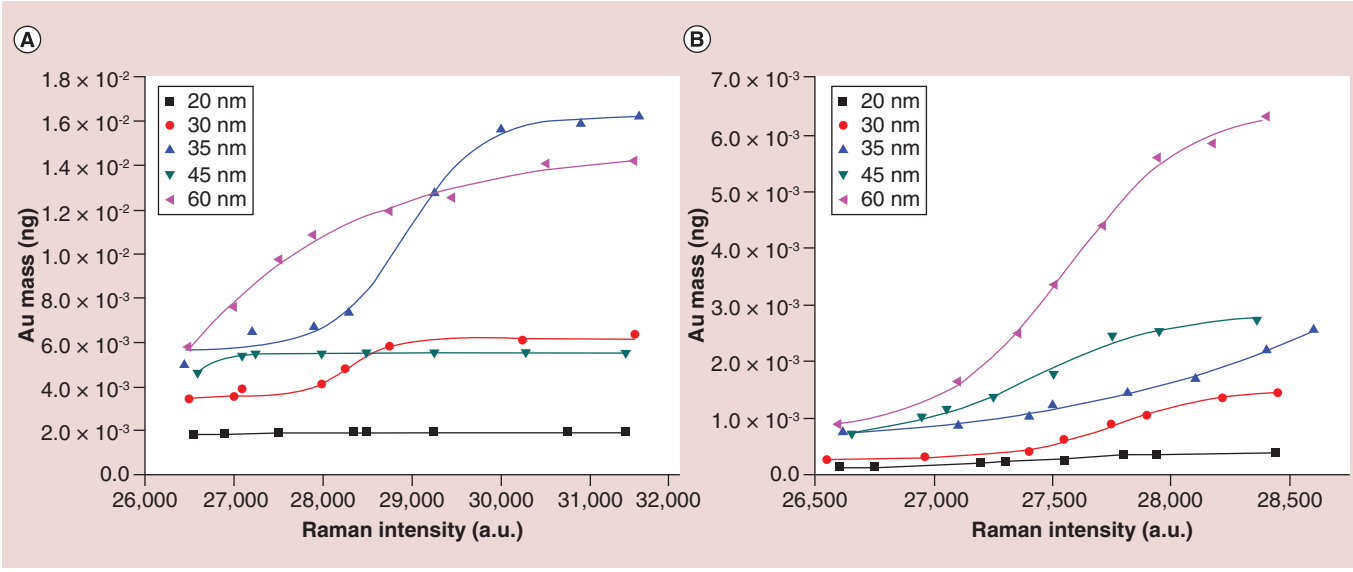

Figure 5. Au mass dependence on the average Raman intensity of the peak at 1576 cm^{-1} in cell. (A) Single HepG2 cell and **(B)** single HL-7702 cell. The data points are arranged according to the incubation time (2, 4, 6, 8. 12.16, 20 and 24 h) from left to right for each curve.
Au: Gold.

being incubated for 12 h. This is similar to the results of previous works on citrate- and herceptin-coated Au NPs in cells [31,32].

In addition, the relation between the cellular uptake and concentration of the Au NPs was investigated and are separately depicted in Figure 7A and B. It is clear that the Au mass in the HL-7702 and HepG2 cells increases with increasing incubation time and concentrations of the Au colloids, respectively. We also find that the Au uptake rate of the HepG2 cells is higher than that of the HL-7702 cells, but it gradually reaches a plateau from the incubation time of 12 h onward. Furthermore, there is a significant variation in the uptake rate for different types of cells. The HepG2 cells obviously showed higher cellular uptake rate than HL-7702 cells.

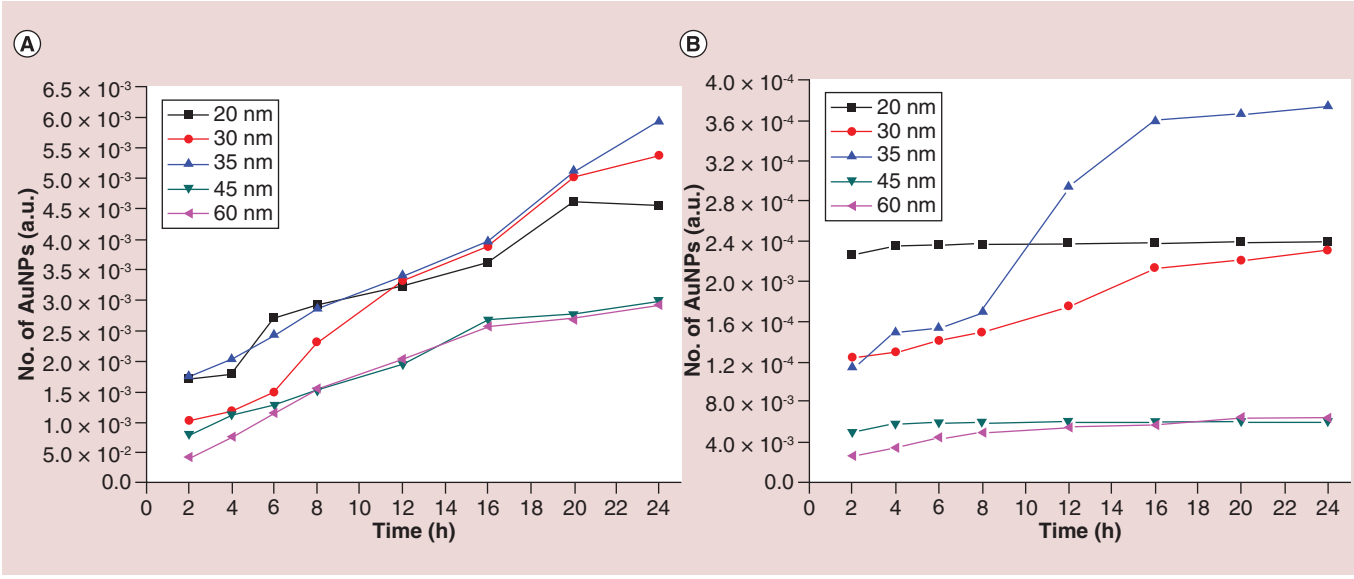

Figure 6. Number of Au NPs variation with the incubation time in cell. (A) Single HL-7702 cell and **(B)** single HepG2 cell.
Au NP: Gold nanoparticle.

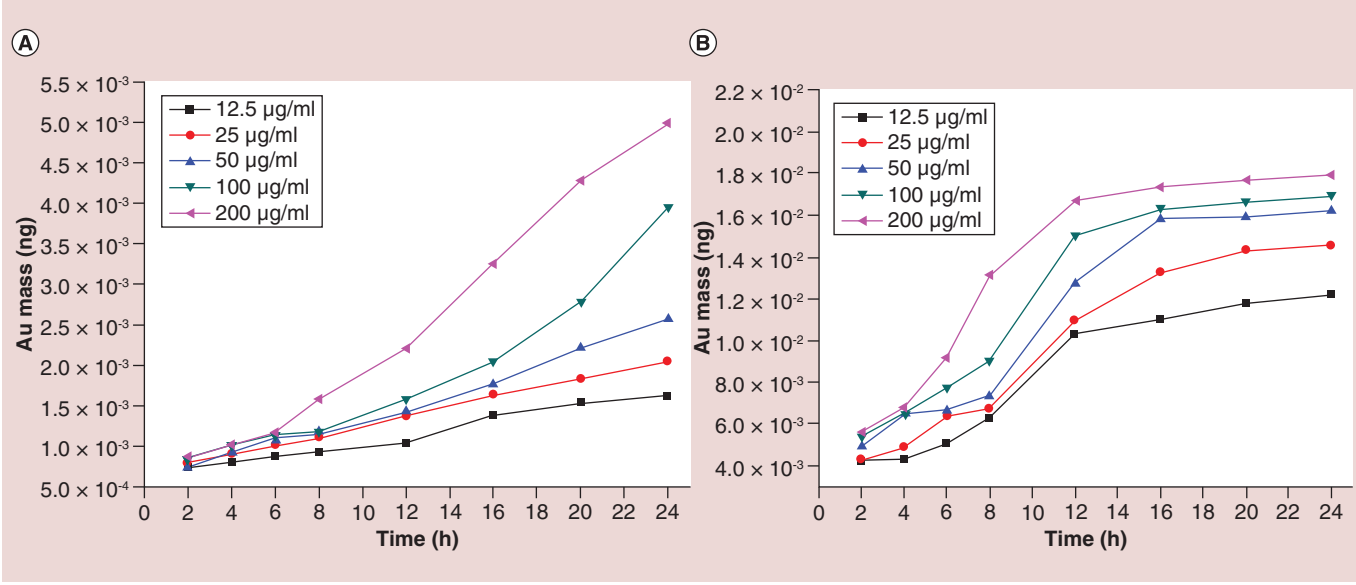

Figure 7. Au mass internalized in cell at different time. Au mass internalized in **(A)** single HL-7702 cell and **(B)** single HepG2 cell varying with the incubation time for Au NPs of 35 nm at different concentrations of Au colloids.
Au: Gold; Au NP: Gold nanoparticle.

Cytotoxicity & PPTT examinations

For achieving an ideal PPTT, a direct solution is the internalization of more number of plasmonic NPs into cancer cells and fewer number into the normal cells, resulting in a rapid death of the cancer cells and a high survival of the normal cells. Here, based on the analysis of the cellular uptake in the previous section, Figure 8A and B display the ratio of the Au mass in single HepG2 and HL-7702 cells for different sizes and concentrations of Au NPs, respectively. From Figure 8A, we find that the largest ratio of Au mass is for 20 nm Au NPs and 2 h of incubation time. However, as shown in Figure 5, the Au mass in both the cells at this time is low, which implies that a stronger laser power or longer exposure time is needed to achieve high-efficiency PPTT. However, we also find a large ratio of 9.08 for 35-nm-Au NPs and 16 h of incubation time and not only is the Au mass in both the cells high but

10.2217/nnm-2018-0126

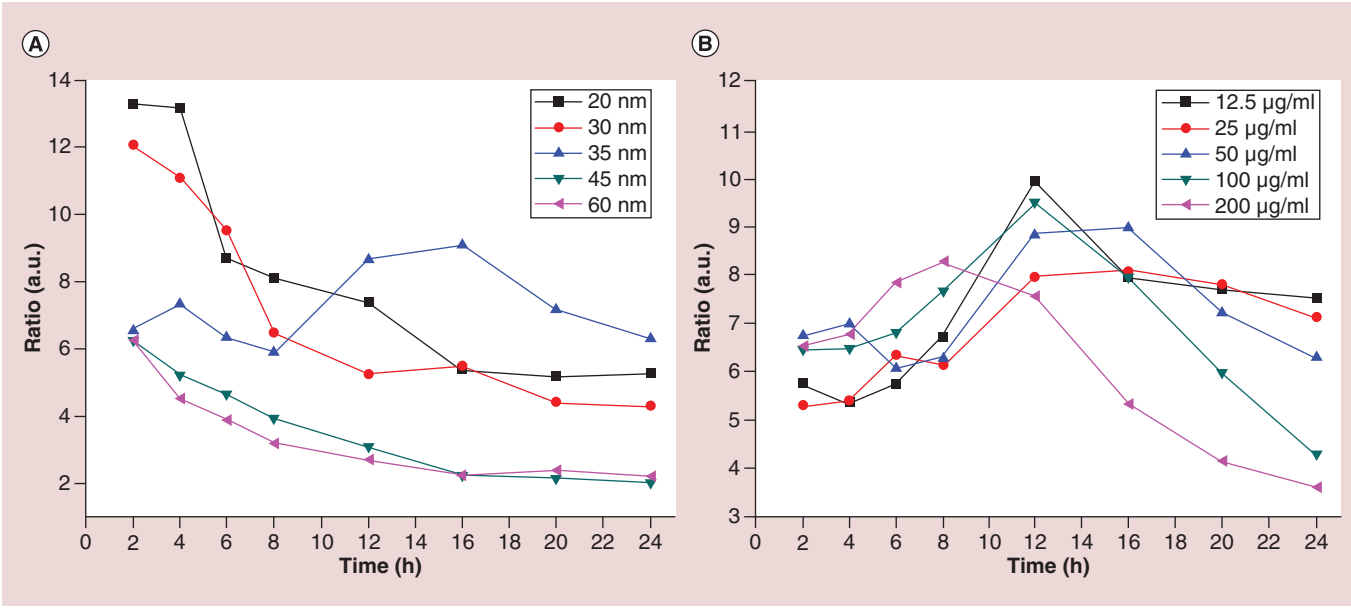

Figure 8. Ratio of the Au mass internalized in single HepG2 and HL-7702 cells. (A) Different sizes of Au NPs at a concentration of 50 μg/ml and **(B)** different concentrations of Au NPs with a size of 35 nm.
Au: Gold; Au NP: Gold nanopartoicle.

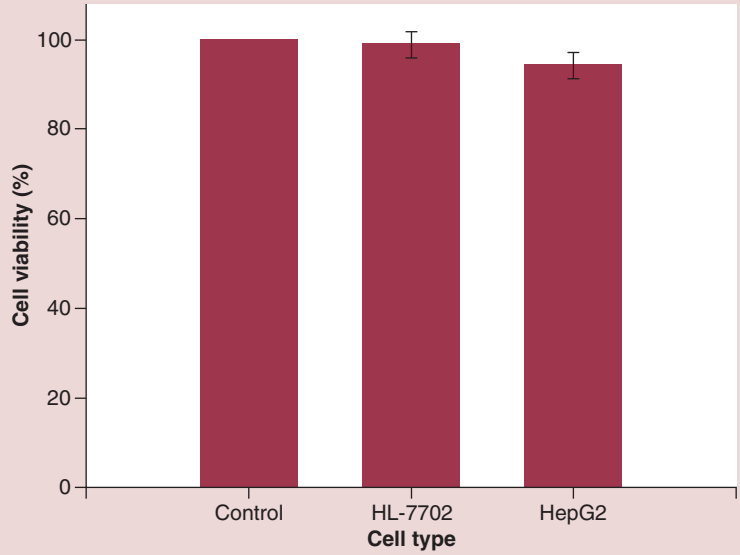

Figure 9. Cytotoxicity of the HL-7702 and HepG2 cells evaluated by methyl thiazolyl tetrazolium assay after incubation with gold nanoparticles for 16 hours.

the difference in the Au masses is also a maximum. Moreover, as shown in Figure 8B, although the ratio of Au mass is large for 12.5 μg/ml of Au NP concentration and 12 h of incubation time, the Au mass in both the cells is relatively low compared with the case of 50 μg/ml of Au NP concentration and 16 h of incubation time. Based on the above analysis, 16 h of incubation time, 35 nm of size and 50 μg/ml of Au NP concentration are selected as the optimal parameters for the subsequent cellular uptake experiments.

The cytotoxicity of the Au NPs is examined by an MTT assay (Table S3 in Supplementary material), and Figure 9 presents the cell viability of the HL-7702 and HepG2 cells for the above selected cellular uptake experiments [20–22].

From Figure 9, we find that the HL-7702 and HepG2 cells exhibit high survival rates, which indicates that there is little damage to both the cells under these specific conditions. Simultaneously, the cell viability examined by MTT is also used to evaluate the effect of the laser on the efficiency of PPTT. Figure 10 depicts the results of the PPTT experiments of the HL-7702 and HepG2 cells as a function of the laser power, exposure time and laser wavelength. In Figure 10A–D, it is seen that the cell viability decreases with the increase in either the exposure time or laser power, and the cell viability of the HL-7702 cells is typically higher than that of the HepG2 cells. Interestingly, the cell viability of the HL-7702 cells under the different conditions is practically higher than 70%, whereas the cell viability of the HepG2 cells is even as low as 30.8% under laser irradiation of 532 nm wavelength, which implies that most of the HL-7702 cells survive, whereas most of the HepG2 cells get damaged. As shown in Figures 10(E–F), the difference between the cell viabilities of both the cells exhibits a maximum at 16 mW of laser power and 4 min of exposure time, respectively. In particular, the difference in the cell viability with irradiation of 532 nm wavelength is larger than that for irradiation of 785 nm wavelength.

Discussion

Based on the developed methodology to evaluate the cellular uptake by combining of Raman mapping and ICP-MS techniques, two groups of calibration curves were established in Figure 5 as a function of the average Raman intensity and the Au mass in single HL-7702 and HepG2 cells. Here, it should be pointing out that the average Raman intensity of the peaks at 1576 cm^{-1} virtually depends on the number of 4MBA linked with Au NPs internalized in single cell. Thus, thermogravimetric experiments were used to exactly quantify the number of 4MBA coated on the Au NPs with different sizes and the result is shown in Figure S3 and Figure S4 of Supplementary material. And from Table S2 in Supplementary material, the number (mass) of 4MBA coated on Au NPs increases as the increase of Au NPs size. In other words, the SERS intensity of 4MBA should increase with the increase of Au NPs size. However, as shown in Figure 5, the average Raman intensity substantially depends on the cellular uptake of Au NPs under different conditions such as size and concentration of Au NPs, including incubation time and cell types, which is consisted with the predicted of references [33,34]. Therefore, Figure 5 really reflects the synthesized effect of cellular uptake of Au NPs.

Moreover, as shown in Figure 6, during the cellular uptake process, we find that the number of Au NPs in both the cells increases from a small to large value to reach a maximum and then it decreases with the increase in the size of the Au NPs, except for the 20 nm Au NPs. Indeed, the efficiency of cellular uptake is mainly dependent on two factors: the amount of free energy required for wrapping the Au NPs and kinetics of the diffusion of the receptors to the binding sites in the cell membrane. If the Au NPs have a small size, fewer receptors will bond with the Au NPs, and consequently, less free energy will be produced to wrap the Au NPs on the surface of the cell membrane. If the size of the Au NPs is large, more receptors will be taken up by the Au NPs, thereby affecting the kinetics of the diffusion of the receptors to the binding sites, in other words, the receptors will be insufficient to be bound, causing the increase of wrapping time [27]. That is why the number of 35 nm size of Au NPs is more than that of other Au NPs in cell. And in Figure 6, the cellular uptake of the Au NPs with size of 20 nm is almost higher than other sizes of AU NPs for entire incubation process, especially for the HL-7702 cells in the early period (before 10 h), which was also suggested by the higher internalization of small Au NPs in HeLa S3 cells [35]. This exhibits that the cellular uptake of small Au NPs highly depends on the cell type. It can be ascribed to two reasons: one is the wrapping of Au NPs of 20 nm size needs less free energy and so more receptors are transferred to the binding sites of the cell membrane; the other is the higher uptake rate of Au NPs of 20 nm size causes the number of Au NPs internalized in the HepG2 cells to reach a maximum in a short time [27,31].

In addition, Figure 7 demonstrated that a high concentration of Au colloids and/or a long incubation time imply penetration of more number of Au NPs into the cellular membrane. Furthermore, there is a significant variation in the uptake rate for HL-7702 and HepG2 cells. This can be attributed to the mitochondrial oxidative phosphorylation in HL-7702 cells and aerobic glycolysis in HepG2 cells [36]. Aerobic glycolysis, also called the Warburg effect, rapidly provides energy and much intermediate products for the uptake and proliferation of cancer cells [37].

In PPTT experiment, the 532 nm of laser caused more damage to both cells compared with 785 nm of laser, which can be ascribed to that the resonance absorption of 35 nm of Au NPs Figure 1F is located at 534 nm and can convert significant heat to cause more cells death. Considering the results of laser power and exposure time, it suggests that 16 mW of laser power, 4 min of exposure time and 532 nm of irradiation wavelength may be the optimal experimental parameters for achieving high-efficiency PPTT.

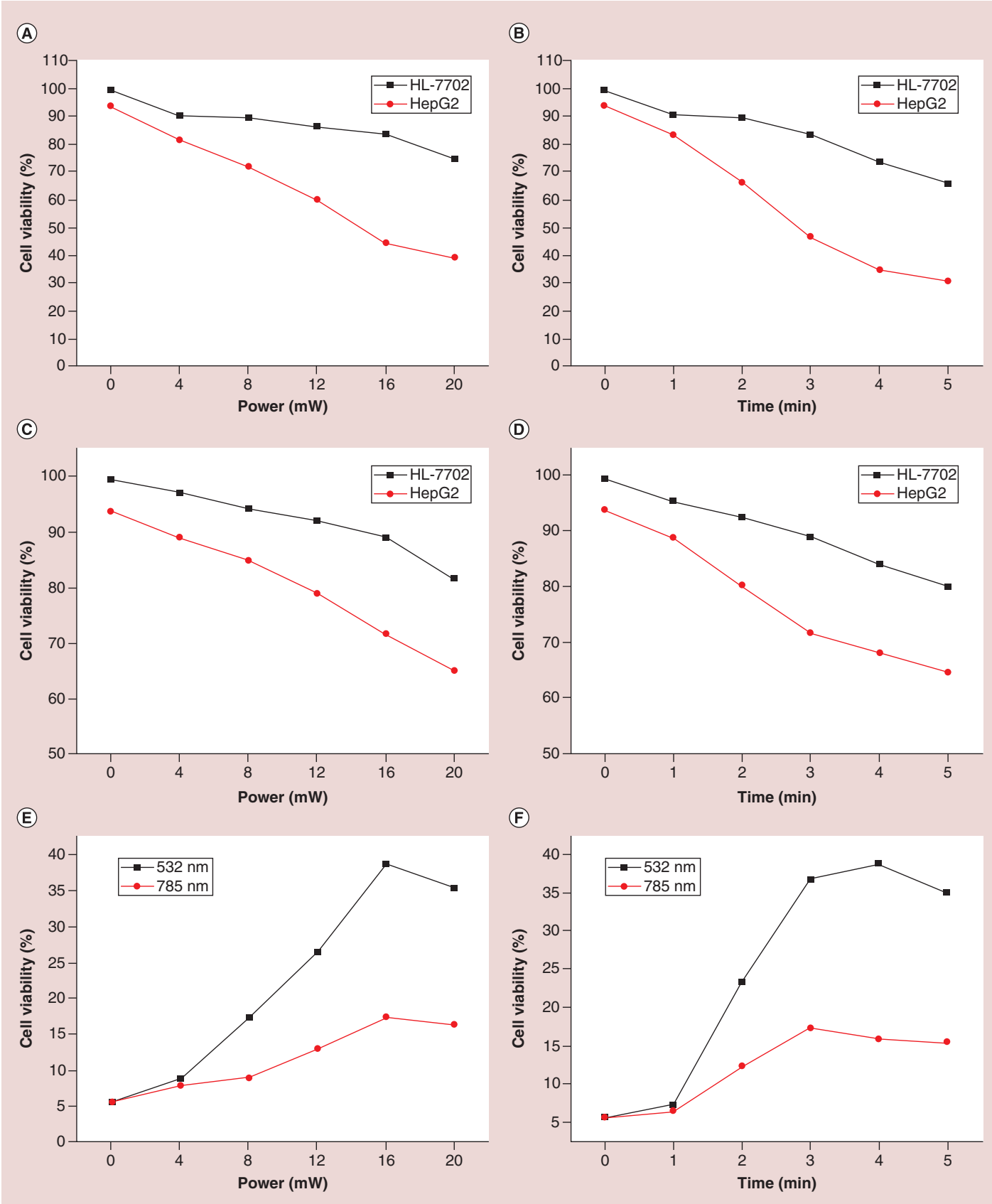

Figure 10. Cell viability of cell. Cell viability of HL-7702 and HepG2 cells after being treated with the laser of 532 nm. **(A)** Under different powers for fixed time of 3 min and **(B)** Under the power of 16 mW for different times; the cell viability of HL-7702 and HepG2 cells after being treated with the laser of 785 nm **(C)** Under different powers for fixed time of 3 min and **(D)** Under the power of 16 mW for different times; **(E–F)** Difference between the cell viabilities of HL-7702 and HepG2 cells presented in **A**, **C** and **B**, **D**, respectively.

Conclusion

In summary, the cellular uptake of Au NPs is investigated by combining the Raman mapping and ICP-MS techniques and the optimal parameters of the Au NPs and laser are determined for achieving high-efficiency PPTT of HL-7702 and HepG2 cells. The results show that the mass of the Au NPs in the cells increases with increasing incubation time, size and concentration of the Au NPs and more Au NPs with a size of 35 nm are internalized in both the cells. Particularly, the Au mass in the HepG2 cells is much larger than that in the HL-7702 cells. This suggests that the cellular uptake is not only affected by the size and concentration of the Au NPs but is also highly affected by the incubation time and cell types. The optimal parameters (16 h of incubation time and 35 nm and 50 μg/ml of Au NPs) are identified for achieving a large ratio of Au mass in both the cells. Furthermore, the optimal experimental conditions for *in vitro* PPTT are determined by adjusting the laser wavelength, laser power and exposure time. This work demonstrates that the cellular uptake of the Au NPs is the most important key for realizing high-efficiency PPTT and provides an effective guide for the development of advanced PPTT.

Future perspective

In our work, the combination of Raman and ICP-MS techniques as a novel method was proposed to quantify the cellular uptake of Au NPs internaized in HL-7702 and HepG2 cells and an efficient PPTT was implemented by adjusting the irradiating conditions of the laser. And many significant results have been obtained by analyzing the role of Au NPs in experimental process, which not only confirm the biological mechanism of cellular uptake, but also show a prior potential application in the clinical therapy of cancer. In the future, a more methodological development of the basic technique should be achieved to effectively guide the explore in the biomedical field, such as the tumor imaging *in vitro* and *in vivo*, drug delivery and photothermal therapy.

Executive summary

- A novel method was developed to quantify the cellular uptake of Au Nanoparticles (Au NPs) by combining Raman mapping and Inductively-coupled plasma mass spectrometry.
- Au NPs were synthesized by an improved Frens' method.
- The cellular uptake of the Au NPs was not only affected by their size and concentration but also by the incubation time and cell type.
- Incubation time of 16 h and Au NPs of 35 nm and 50 μg/mL were chosen as the optimal parameters to realize a large ratio of the Au mass in HL-7702 and HepG2 cells.
- High-efficiency Plasmonic photothermal therapy was achieved *in vitro* and exhibited a large difference between the cell viabilities of the HepG2 and HL-7702 cells, which indicated a potential application prospect in the treatment of cancer *in vivo*.

Supplementary data

To view the supplementary data that accompany this paper please visit the journal website at: www.futuremedicine.com/doi/full/10.2217/nnm-2018-0126

Financial & competing interests disclosure

This work was supported by the National Natural Science Foundation of China (Grant numbers: 61320106014 and 61675104) and K. C. Wong Magna Fund in Ningbo University, China. The authors have no other relevant affiliations or financial involvement with any organization or entity with a financial interest in or financial conflict with the subject matter or materials discussed in the manuscript apart from those disclosed.

No writing assistance was utilized in the production of this manuscript.

References

Papers of special note have been highlighted as: • of interest; •• of considerable interest

1. Gu Q, Zhao H, Xu B, J X, Lv J. Photothermal modeling of plasmonic nanostructures: a review. *Nanosci. Nanotech. Let.* 9(5), 599–608 (2017).

• **Good review for introducing plasmonic photothermal therapy.**

2. Li JL, Tang B, Yuan B, Sun L, Wang XG. A review of optical imaging and therapy using nanosized graphene and graphene oxide. *Biomaterials* 34(37), 9519–9534 (2013).
3. Jain PK, Huang X, El-Sayed IH, El-Sayed MA. Noble metals on the nanoscale optical and photothermal properties and some applications in imaging, sensing, biology and medicine. *Accounts Chem. Res.* 41(12), 1578–1586 (2008).
4. Liu Y, Ashton JR, Moding EJ *et al.* A plasmonic gold nanostar theranostic probe for *in vivo* tumor imaging and photothermal therapy. *Theranostics* 5(9), 946 (2015).
5. Hainfeld JF, O'Connor MJ, Lin P, Qian L, Slatkin DN, Smilowitz HM. Infrared-transparent gold nanoparticles converted by tumors to infrared absorbers cure tumors in mice by photothermal therapy. *PLoS ONE* 9(2), e88414 (2014).
6. Huang X, Jain PK, El-Sayed IH, El-Sayed MA. Plasmonic photothermal therapy (PPTT) using gold nanoparticles. *Lasers Med. Sci.* 23(3), 217–228 (2008).
7. Riley RS, Day ES. Gold nanoparticle-mediated photothermal therapy: applications and opportunities for multimodal cancer treatment. *Wires. Nanomed. Nanobi* 9(4), e1449 (2017).
8. Huang WC, Tsai PJ, Chen YC. Functional gold nanoparticles as photothermal agents for selective-killing of pathogenic bacteria. *Nanomedicine* 2(6), 777–787 (2007).
9. Black KC, Yi J, Rivera JG, Zelasko-Leon DC, Messersmith PB. Polydopamine-enabled surface functionalization of gold nanorods for cancer cell-targeted imaging and photothermal therapy. *Nanomedicine* 8(1), 17–28 (2013).
10. Rengan AK, Bukhari AB, Pradhan A *et al. In vivo* analysis of biodegradable liposome gold nanoparticles as efficient agents for photothermal therapy of cancer. *Nano Lett.* 15(2), 842–848 (2015).
11. Zhao F, Zhao Y, Liu Y, Chang X, Chen C, Zhao Y. Cellular uptake, intracellular trafficking and cytotoxicity of nanomaterials. *Small* 7(10), 1322–1337 (2011).

•• **An insightful article about the cellular uptake.**

12. Rosman C, Pierrat S, Henkel A *et al.* A new approach to assess gold nanoparticle uptake by mammalian cells: combining optical dark-field and transmission electron microscopy. *Small* 8(23), 3683–3690 (2012).
13. Guehrs E, Schneider M, Gunther CM *et al.* Quantification of silver nanoparticle uptake and distribution within individual human macrophages by FIB/SEM slice and view. *J. Nanobiotechnol.* 15(1), 21 (2017).
14. Gliga AR, Skoglund S, Odnevall W, Fadeel B, Karlsson HL. Size-dependent cytotoxicity of silver nanoparticles in human lung cells the role of cellular uptake, agglomeration and Ag release. *Part. Fibre Toxicol.* 11(1), 11 (2014).
15. Salvati A, Aberg C, Dos Santos T *et al.* Experimental and theoretical comparison of intracellular import of polymeric nanoparticles and small molecules: toward models of uptake kinetics. *Nanomedicine* 7(6), 818–826 (2011).
16. Hsiao IL, Bierkandt FS, Reichardt P *et al.* Quantification and visualization of cellular uptake of TiO2 and Ag nanoparticles: comparison of different ICP-MS techniques. *J. Nanobiotechnol.* 14(1), 50 (2016).

• **A good paper for introducing the inductively coupled plasma-mass spectrometry techniques.**

17. Abramczyk H, Brozek-Pluska B. Raman imaging in biochemical and biomedical applications. diagnosis and treatment of breast cancer. *Chem. Rev.* 113(8), 5766–5781 (2013).

• **A good paper for introducing the Raman imaging.**

18. Luo R, Li Y, Zhou Q *et al.* SERS monitoring the dynamics of local pH in lysosome of living cells during photothermal therapy. *Analyst* 141(11), 3224–3227 (2016).
19. Frens G. Controlled nucleation for the regulation of the particle size in monodisperse gold suspensions. *Nature* 241(105), 20 (1973).

• **An important article about synthesizing gold nanoparticles.**

20. Osman IF, Baumgartner A, Cemeli E, Fletcher JN, Anderson D. Genotoxicity and cytotoxicity of zinc oxide and titanium dioxide in HEp-2 cells. *Nanomedicine* 5(8), 1193–1203 (2010).
21. Lopes VR, Loitto V, Audinot JN, Bayat N, Gutleb AC, Cristobal S. Dose-dependent autophagic effect of titanium dioxide nanoparticles in human HaCaT cells at noncytotoxic levels. *J. Nanobiotechnol.* 14(1), 22 (2016).
22. Wentzel JF, Lombard MJ, Plessis LHD, Zandberg L. Evaluation of the cytotoxic properties, gene expression profiles and secondary signalling responses of cultured cells exposed to fumonisin B1, deoxynivalenol and zearalenone mycotoxins. *Arch. Toxicol.* 91(5), 2265–2282 (2017).
23. Michota A, Bukowska J. Surface-enhanced Raman scattering (SERS) of 4-mercaptobenzoic acid on silver and gold substrates. *J. Raman Spectrosc.* 34(1), 21–25 (2003).
24. Xu Y. Chapter-2: Proteins. *Raman spectroscopy in application of structure biology* Chemical Industry Press, Beijing, China, 12–102 (2005).

25. Coradeghini R, Gioria S, Garcia CP *et al.* Size-dependent toxicity and cell interaction mechanisms of gold nanoparticles on mouse fibroblasts. *Toxicol. Lett.* 217(3), 205–216 (2013).

- **A good paper for introducing the cytotoxicity.**

26. Albanese A, Chan WCW. Effect of gold nanoparticle aggregation on cell uptake and toxicity. *ACS Nano* 5(7), 5478–5489 (2011).

27. Chithrani BD, Chan WCW. Elucidating the mechanism of cellular uptake and removal of protein-coated gold nanoparticles of different sizes and shapes. *Nano Lett.* 7(6), 1542–1550 (2007).

28. Kettler K, Veltman K, Meent DVD, Wezel AV, Hendriks AJ. Cellular uptake of nanoparticles as determined by particle properties, experimental conditions and cell type. *Environ. Toxicol. Chem.* 33(3), 481–492 (2014).

29. Yameen B, Choi WI, Vilos C, Swami A, Shi J, Farokhzad OC. Insight into nanoparticle cellular uptake and intracellular targeting. *J. Control Release* 190, 485–499 (2014).

30. Beddoes CM, Case CP, Briscoe WH. Understanding nanoparticle cellular entry: a physicochemical perspective. *Adv. Colloid interface Sci.* 218, 48–68 (2015).

- **A good article for introducing the nanoparticle cellular entry.**

31. Chithrani BD, Ghazani AA, Chan WCW. Determining the size and shape dependence of gold nanoparticle uptake into mammalian cells. *Nano Lett.* 6(4), 662–668 (2006).

32. Jiang W, Kim BYS, Rutka JT, Chan WCW. Nanoparticle-mediated cellular response is size-dependent. *Nat. Nanotechnol.* 3(3), 145–150 (2008).

33. Salatin S, Dizaj SM, Khosroushahi AY. Effect of the surface modification, size and shape on cellular uptake of nanoparticles. *Cell Biol. Int.* 39(8), 881–890 (2015).

34. Banerjee A, Qi J, Gogoi R, Wong J, Mitragotri S. Role of nanoparticle size, shape and surface chemistry in oral drug delivery. *J. Control Release* 238, 176–185 (2016).

35. Xu C, Tung GA, Sun S. Size and concentration effect of gold nanoparticles on x-ray attenuation as measured on computed tomography. *Chem. Mater.* 20(13), 4167–4169 (2008).

36. Warburg O, Wind F, Negelein E. The metabolism of tumors in the body. *J. Gen. Physiol.* 8(6), 519 (1927).

- **An important article related to the Warburg effect.**

37. Vander Heiden MG, Cantley LC, Thompson CB. Understanding the Warburg effect: the metabolic requirements of cell proliferation. *Science* 324(5930), 1029–1033 (2009).